

Technical Results from the Surface Run of the LUX Dark Matter Experiment

D. S. Akerib^b, X. Bai^h, E. Bernard^p, A. Bernstein^e, A. Bradley^b, D. Byram^o,
S. B. Cahn^p, M. C. Carmona-Benitez^b, J. J. Chapman^a, T. Coffey^b, A. Dobi^m,
E. Dragowsky^b, E. Druszkiewiczⁿ, B. Edwards^p, C. H. Faham^a, S. Fiorucci^a,
R. J. Gaitskell^a, K. R. Gibson^{b,*}, M. Gilchriese^j, C. Hall^m, M. Hanhardt^h,
M. Ihm^j, R. G. Jacobsen^j, L. Kastens^p, K. Kazkaz^e, R. Knoche^m, N. Larsen^p,
C. Lee^b, K. T. Lesko^d, A. Lindote^f, M. I. Lopes^f, A. Lyashenko^p,
D. C. Mallin^a, R. Manninoⁱ, D. N. McKinsey^p, D. Mei^o, J. Mock^k,
M. Moongweluwanⁿ, M. Morii^c, H. Nelson^l, F. Neves^f, J. A. Nikkel^p,
M. Pangilinan^a, K. Pech^b, P. Phelps^b, A. Rodionovⁱ, T. Shutt^b, C. Silva^f,
W. Skulskiⁿ, V. N. Solovov^f, P. Sorensen^e, T. Stieglerⁱ, M. Sweany^k,
M. Szydagis^k, D. Taylor^j, M. Tripathi^k, S. Uvarov^k, J. R. Verbus^a,
L. de Viveiros^f, N. Walsh^k, R. Webbⁱ, J. T. Whiteⁱ, M. Wlasenko^c,
F. L. H. Wolfsⁿ, M. Woods^k, C. Zhang^o

^a*Brown University, Dept. of Physics, 182 Hope St., Providence, RI 02912*

^b*Case Western Reserve University, Dept. of Physics, 10900 Euclid Ave, Cleveland, OH 44106*

^c*Harvard University, Dept. of Physics, 17 Oxford St., Cambridge, MA 02138*

^d*Lawrence Berkeley National Laboratory, 1 Cyclotron Rd., Berkeley, CA 94720*

^e*Lawrence Livermore National Laboratory, 7000 East Ave., Livermore, CA 94551*

^f*LIP-Coimbra, Department of Physics, University of Coimbra, Rua Larga, 3004-516 Coimbra, Portugal*

^g*Moscow Engineering Physics Institute, 31 Kashirskoe shosse, Moscow 115409*

^h*South Dakota School of Mines and Technology, 501 East St Joseph St., Rapid City, SD 57701*

ⁱ*Texas A & M University, Dept. of Physics, College Station, TX 77843*

^j*University of California Berkeley, Dept. of Physics, Berkeley, CA 94720-7300*

^k*University of California Davis, Dept. of Physics, One Shields Ave., Davis, CA 95616*

^l*University of California Santa Barbara, Dept. of Physics, Santa Barbara, CA 95616*

^m*University of Maryland, Dept. of Physics, College Park, MD 20742*

ⁿ*University of Rochester, Dept. of Physics and Astronomy, Rochester, NY 14627*

^o*University of South Dakota, Dept. of Physics, 414E Clark St., Vermillion, SD 57069*

^p*Yale University, Dept. of Physics, 217 Prospect St., New Haven, CT 06511*

*Corresponding Author: karen.gibson@case.edu

Abstract

We present the results of the three-month above-ground commissioning run of the Large Underground Xenon (LUX) experiment at the Sanford Underground Research Facility located in Lead, South Dakota, USA. LUX is a 370 kg liquid xenon detector that will search for cold dark matter in the form of Weakly Interacting Massive Particles (WIMPs). The commissioning run, conducted with the detector immersed in a water tank, validated the integration of the various sub-systems in preparation of the underground deployment. Using the data collected, we report excellent light collection properties, achieving 8.4 photoelectrons per keV for 662 keV electron recoils without an applied electric field, measured in the center of the WIMP target. We also find good energy and position resolution in relatively high-energy interactions from a variety of internal and external sources. Finally, we have used the commissioning data to tune the optical properties of our simulation and report updated sensitivity projections for spin-independent WIMP-nucleon scattering.

Keywords:

Liquid xenon detectors, Dark matter, WIMP, Direct detection

1. Introduction

The goal of the LUX experiment is to detect or exclude WIMP-nucleon elastic scattering interactions [1] with scalar cross sections of $7 \times 10^{-46} \text{ cm}^2$ [2] at a WIMP mass of $100 \text{ GeV}/c^2$, equivalent to 0.5 events/100 kg/month in the inner 100 kg fiducial volume of the 370 kg liquid xenon (LXe) detector.

Events in the LXe target create direct scintillation light (S1), while electrons escaping recombination at the event site are drifted to the liquid surface and extracted into the gas phase by applied electric fields, where they create electroluminescent light (S2) (see Ref. [3] for a comprehensive review of these processes). Both S1 and S2 processes emit vacuum-ultraviolet (VUV) light peaking at 178 nm. The dominant backgrounds to the WIMP search consist of nuclear recoils, due to neutrons, and electron recoils, primarily from external γ -rays and internal β decays. Local external backgrounds are minimized by the appropriate choice of detector materials, including radio-pure titanium for the cryostat and low-radioactivity photomultipliers (PMTs) for light readout, and the inclusion of water shielding around the detector. In addition, two data analysis methods help to discriminate against the remaining background: (i) separation of electron recoil interactions from nuclear recoils, based on the amount of S2 light relative to S1 light; and (ii) the strong self-shielding capability of the dense LXe that, when coupled with the use of three-dimensional event reconstruction, significantly reduces the electromagnetic and neutron backgrounds that occur primarily in the outermost LXe. As in most direct search detectors, WIMP interactions are indistinguishable from single elastic neutron scatters in LUX, so great care must be taken to minimize the number of neutrons propagating to the fiducial region of the LXe chamber.

The LUX experiment will begin to search for WIMP dark matter in the Davis campus at the 4850-foot level (1480 m) of the Sanford Underground Research Facility (SURF) in late 2012. The underground deployment of such an experiment is a complex process and a major goal of the surface run was

to validate the various sub-systems and to verify the integration of the entire system. Some LUX components involve novel technical solutions that benefited from realistic testing, including the cooling, gas circulation and purification systems, the control and safety systems, high voltage delivery, and the data acquisition system. Conducting the detector commissioning above ground also allowed corrective actions to be implemented more effectively prior to underground running. A second aim of the run was to allow a preliminary assessment of the radiation-detection performance of the experiment. Besides early validation of key design parameters, such as the light collection of the chamber, this also exercised the general data analysis procedures, including the reconstruction of LXe interactions from a variety of radioactive sources. While rigorous characterization of the low-energy performance of the experiment can only be carried out in the low-background environment of an underground laboratory, these complex data analysis procedures require substantial development, and the early data from this run has proved to be very valuable in advancing the analysis effort.

This article is organized as follows. We discuss the experimental set-up for the surface run, the performance of the integrated system, and surface data-taking in Section 2. Measurements of the light and charge responses for high-energy background and calibration sources are presented in Section 3. The outlook for the LUX dark matter search, based on the results presented here, is discussed in Section 4.

2. LUX detector commissioning

The commissioning of the LUX detector was conducted at a multi-level surface facility outfitted by SURF for this purpose, depicted schematically in Fig. 1. The detector was deployed for full commissioning during August 2011; the system-integrated commissioning began on September 1, 2011, and extended through February 14, 2012, with more than 100 days of cryogenic detector operation. During the surface run, the detector was filled with 370 kg of xenon, with 300 kg in the active region between the cathode and anode wire planes. The surface facility lies 1.6 km above sea level and has higher cosmic-related backgrounds than are found at sea level. In order to test all aspects of the underground detector deployment and to reduce γ and neutron backgrounds during data-taking, the detector was operated within a 3 m diameter water tank designed for commissioning. The water tank provided approximately 1 m of shielding around the cryostat and reduced the total γ -ray background, which is largely due to the concrete and wood building materials used in the surface facility, from 10 kHz to 100 Hz. The water shield also reduced the cosmic-ray-induced neutron background from 240 Hz to 10 Hz. The 108.8 ± 0.3 Hz muon background measured at the surface lab is not significantly affected by the shield.

The LUX experiment is described in detail in Ref. [4]. The LUX detector is a cylindrical two-phase xenon time-projection chamber (TPC), with instrumented xenon covering 55 cm in the vertical (z) direction and 24 cm in radial extent. The xenon scintillation light is detected with 122 VUV Hamamatsu R8778 photomultiplier tubes (PMTs) evenly divided between top and bottom arrays, operating within the gas and liquid phases, respectively, and

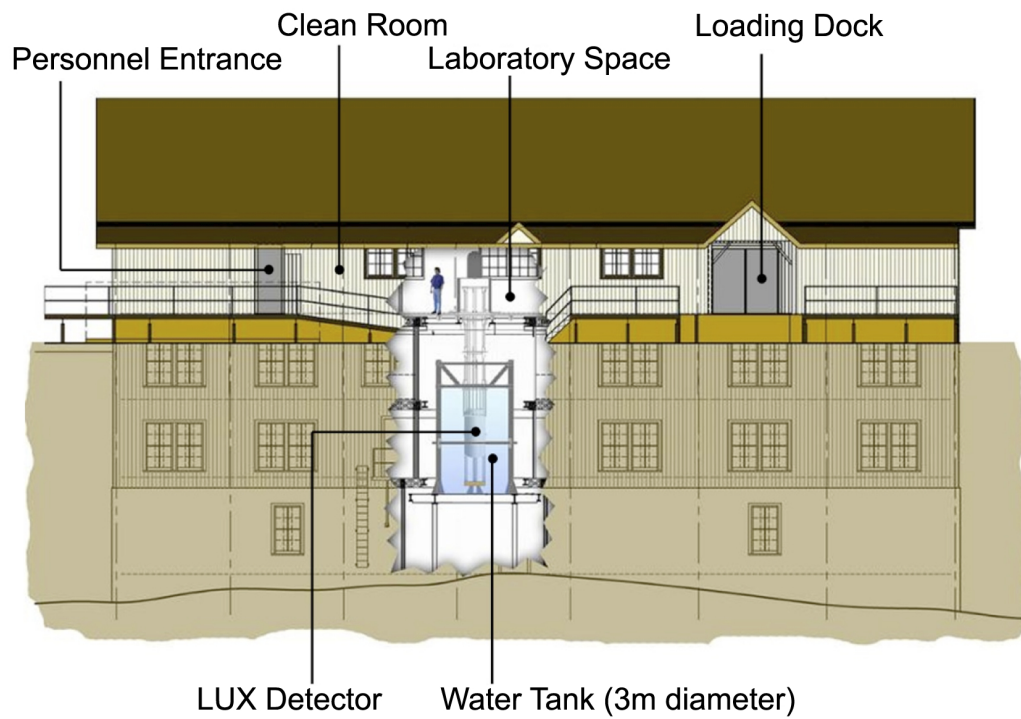


Figure 1: A cutaway of the surface facility provided by SURF for LUX detector commissioning is shown. All detector systems were tested above ground, including detector deployment in a 3 m diameter water shield.

held in place with copper support structures. The VUV scintillation light is reflected by twelve polytetrafluoroethylene (PTFE) panels [5] that fully cover the length of the active region and additional PTFE reflectors that cover all copper surfaces in the PMT support structures. The PTFE panels are 1 cm thick in the radial direction and are mounted on a polyethylene support structure. The cryostat is fully immersed in the water shield and all electrical and gas connections are made through conduits that emerge from the top of the cryostat and lead to a cart located on the experimental deck.

To extract ionization from interaction sites and produce S2 light, an electric field is applied along the z -axis of the detector using four wire planes and an anode wire-mesh plane. The field between the cathode and gate wire planes is used to drift the electrons vertically through the liquid xenon, away from the event site and toward the gas gap above the gate wire plane (hereafter called the “drift field”). The field between the gate wire plane and the anode mesh plane then extracts the ionization electrons into a layer of gas, approximately 5 mm thick, where they generate S2 light before being collected on the anode mesh; the terms “extraction field” and “electroluminescence field” apply just below and above the liquid surface, respectively. Additional wire planes are included above the bottom PMT bank and below the top PMT bank to terminate the field lines and shield the PMT optics. Data taken without an applied electric field provides only S1 light. “Dual-phase” data, which is taken with applied electric fields, produces S1 light in the liquid xenon and S2 light in the layer of gaseous xenon between the liquid surface and anode mesh plane.

2.1. Detector operation

Detector cooling from room temperature to 185 K was achieved in eleven days through the use of a liquid nitrogen thermosyphon system [6]. During initial cooling, a maximum cooling rate of 0.8 K/hr was allowed. Although the thermosyphons could deliver a significantly higher rate of cooling, this would risk establishing thermal gradients that could lead to warping of the PTFE panels. Following the initial detector cooling, a stable operating temperature of approximately 175 K was achieved, although variations in the detector temperature between mid-November and mid-February occurred due to operational changes in the xenon circulation. The detector pressure was stable within 0.3% during at least one four-day period of minimal configuration changes over the New Year holiday.

During surface commissioning, we observed a limitation in the drift field from the onset of electroluminescent discharge on the cathode grid wires at 10 kV. This cathode grid had 10 mm wire spacing and a wire diameter of 100 μm . We had also established a limitation of the cathode high-voltage feedthrough to 20 kV and a very conservative operating field of 62 V/cm, corresponding to an electron drift velocity of 1.2 mm/ μs , was used during dual-phase data taking. A maximum operating field of 120 V/cm was achieved, but we chose to operate at half of that field to remain well within a safe range. In order to address these issues, both the cathode wire plane and the feedthrough were redesigned and new bench-tested versions manufactured ahead of underground deployment, which should enable LUX to operate at a nominal field of 800 V/cm.

The purification system is designed to circulate the xenon gas through a

heated zirconium getter, with the help of an external pump, which requires returning the xenon to the gas phase and re-condensing it [7]. Following the initial liquefaction, it was discovered that an internal plumbing fitting in the circulation line, designed to transfer condensed xenon to the bottom of the detector, came loose during assembly, and the intended xenon circulation path was compromised during the remainder of the surface commissioning. Consequently, xenon purification was explored in several circulation modes over a period of 46 days, including convection and circulating through a plumbing line intended for liquid recovery. Using the original circulation path with the loose fitting, we were able to circulate xenon through the gas handling system at a rate of 35 slpm, corresponding to 300 kg/day, with a net heat load < 5 W. During xenon circulation, the purity of the gas prior to getter purification was monitored with a cold-trap-enhanced mass spectrometer technique [8], and impurity concentrations of 0.4 ppb O_2 and 0.5 ppb N_2 were obtained. The maximum electron drift length achieved within the chamber, which gives a measure of the reduction of electronegative impurities, was 25 cm (200 μs mean electron lifetime). This corresponds to half the length of the active region between the cathode and gate wire planes. This measurement is discussed further in Section 3.1.

2.2. Surface data-taking

We collected zero-field data regularly between mid-November 2011, when we began to condense xenon in the detector, and mid-February 2012, when the surface commissioning ended to prepare the detector for transport underground. Dual-phase data were collected between mid-December and mid-February. The data were recorded through the full data-acquisition (DAQ)

chain, providing the opportunity to assess the performance of the system from beginning to end and to debug all features of the electronics chain and data-taking that could otherwise cause pathologies in the dark matter search data.

A detailed description of the data acquisition system can be found in Ref. [9]. The analog signal is digitized at an operational sampling rate of 100 MHz by Struck ADC modules. Only candidate pulses that pass above a hardware threshold are digitized (called “pulse-only digitization” or POD) in order to reduce the recorded event size by a factor of fifteen, while preserving full sensitivity to dark matter signals. The POD recorded 24 samples before the signal threshold for pulse detection was crossed. We also recorded an additional 31 trailing samples after the pulse dropped below a second threshold, which was consistent with the measured electronics baseline noise and that defined the end of the pulse. For most surface data collected, a pulse detection threshold of 1.5 mV was used. The efficiency of noise rejection using zero suppression was measured by setting a threshold for the POD corresponding to a 95% efficiency to detect single photoelectrons (phe) at nominal PMT gains, while biasing the PMTs to only -100 V and grounding the wire planes. This allowed us to test for noise in the electronics chain, independent of any noise nominally caused by the PMTs being at full bias voltage. We obtained a zero suppression efficiency $> 99.999\%$ in this configuration. During surface operation, the DAQ was able to handle a 1.7 kHz acquisition rate during dual-phase operation without any dead time in downloading data.

The LUX trigger system, described in Ref. [4], was configured to trigger on either S1 or S2 signals for the surface data-taking. The trigger consists of two

8-channel digital signal processors (DDC-8DSP). Sixteen trigger groups are defined, with each group consisting of eight PMTs located in either the top or bottom PMT array. Digital filters are used to search for S1 and S2 signals in the analog sum of the signals in the PMT groups. The multiplicity of the S1 and S2 signals, with pulse areas between a lower and an upper limit, was used to generate triggers. All of the data shown in this paper were collected with an S1 trigger. Events were defined within a window of 500 μs following the S1 trigger, which allowed the collection of pulses along the full length of the detector. Double-triggering was prevented by a trigger hold-off for the 500 μs following a trigger. This mode of operation is different from that planned for underground operation, which will allow multiple triggers in an event.

Muons were a significant source of background during the surface data-taking, with a flux of $0.019 \pm 0.003 \text{ cm}^{-2}\text{s}^{-1}$ measured at the surface facility, which is approximately 14% higher than the value at sea level. At the 4850-foot underground level of SURF, the muon flux is reduced to $(4.4 \pm 0.1) \times 10^{-9} \text{ cm}^{-2}\text{s}^{-1}$ [10] (~ 4 muons per day across the active region of the LUX detector), which corresponds to $4.3 \pm 0.2 \text{ km}$ of water equivalent shielding. For our dark matter search, we require single phe sensitivity in the PMTs and DAQ electronics and both have been designed to operate in a low background environment, with small average VUV photon rates generated within the chamber. Consequently, the electronics chain was optimized to provide single phe sensitivity when operating at a PMT gain of 4×10^6 , but not at PMT gains significantly lower than this. Since cosmic muons can deposit large amounts of energy in the detector, particularly during data-taking with

both S1 and S2 light, we limited both the PMT gain and the extraction and electroluminescence fields between the gate and anode wire planes to safeguard the PMTs during data-taking above ground. Consequently, the PMT gains were limited to 1×10^5 during dual-phase data taking. The DAQ readout configuration for these data required a PMT pair above the nominal POD threshold at 1.5 mV. At the lower gain, this threshold impairs our ability to reconstruct pulses with areas lower than approximately 20 phe for S1 pulses and 500 phe for S2 pulses and produces a non-trivial threshold effect that is not readily de-convolved from the data. Consequently, this acquisition mode does not allow sensible energy reconstruction $\lesssim 100$ keV. During zero-field data taking, which was used to study the light collection properties of the detector, the PMTs were operated at full gain, with sensitivity to single phes at 95% efficiency, and the data did not suffer from an effective low-energy readout threshold.

Digitized pulse shapes are parameterized by a number of characteristic quantities, such as pulse area, height, and length, that can be used to identify S1 and S2 signals. The LXe scintillation mechanism leads to near-exponential VUV pulses with time constants of a few tens of nanoseconds and very fast rise times [11, 12]. Conversely, S2 signals generated by electrons emitted from the liquid surface are typically much larger and have durations of about 1 μ s, due to the drift time of the electrons in the gas gap as well as the smearing of emission times caused by electron diffusion in the liquid. These characteristics allow a clear separation between S1 and S2 pulses. A typical event from the surface run is shown in Fig. 2. We have checked the reconstruction of the pulses and timing information with a number of basic measurements,

including the muon lifetime, shown in Fig. 3. This is measured in the decay of $\mu^+ \rightarrow \bar{\nu}_\mu \nu_e e^+$ using the measured time difference between an S1 signal characteristic of a muon and a subsequent S1 signal. This measurement was made in zero-field data and did not take pile-up into account. We find good agreement between our measured value of 2.18 ± 0.02 (stat.) μs and the world average of $2.197 \mu\text{s}$ [13].

2.3. Preparations for underground running

During the surface commissioning, valuable experience in detector assembly and deployment, operation, and data-taking was gained. We were also able to identify a handful of issues that we rectified prior to the detector transport underground. The inherent limitation in the high-voltage delivery system was solved by a new feed-through that has been developed and tested extensively at 100 kV. A new cathode wire plane with 0.5 cm wire spacing and a wire diameter of $206 \pm 1 \mu\text{m}$ has been assembled and installed. Based on these improvements, we aim to achieve 800 V/cm in the drift region during underground operation, although 500 V/cm will provide adequate discrimination to reach our sensitivity goal [14]. We have upgraded the circulation system to achieve even higher flow rates by ensuring that all fittings are properly connected in the plumbing system and implementing a series of checks that help to ensure the integrity of the detector internal circulation lines prior to full detector deployment. Even without these additional improvements, the LUX detector surface operation was very successful, demonstrating good thermal control, a high gas flow rate through the purification system, and excellent readout capability.

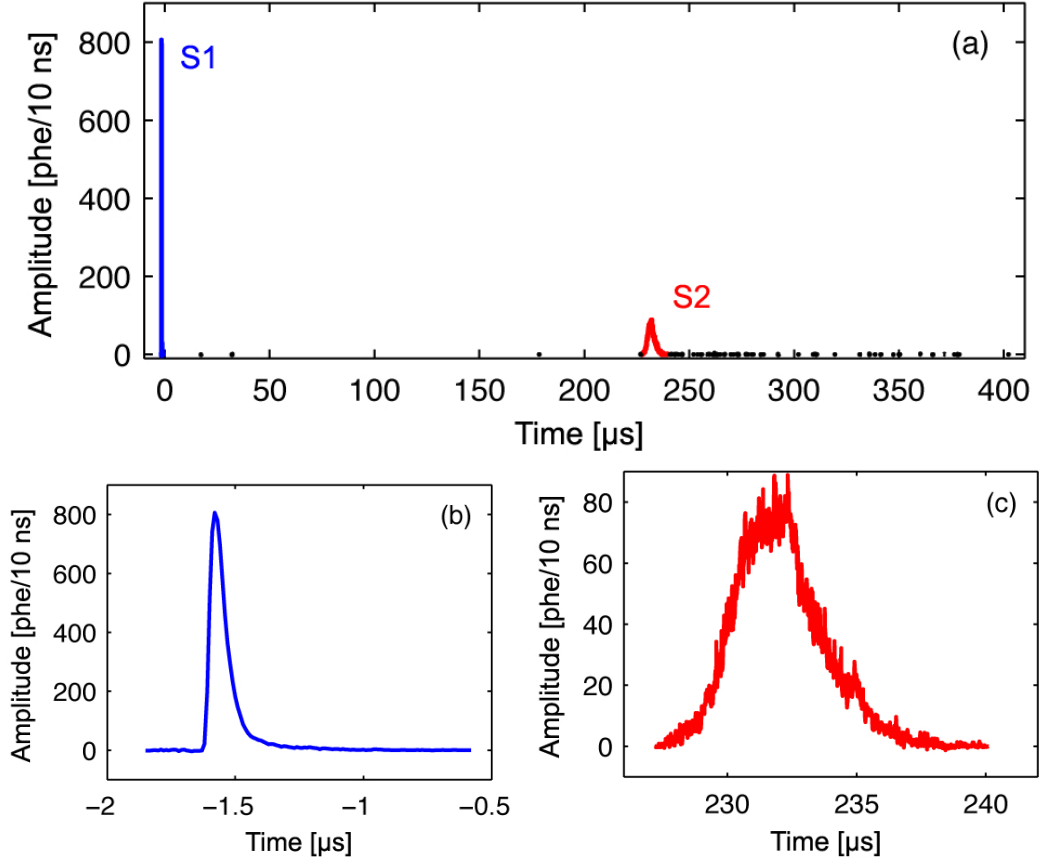


Figure 2: Example dual-phase γ event at 28 cm depth from background data. The entire event is shown in (a), while (b) shows a zoomed view of the S1 signal and (c) shows a zoomed view of the S2 signal. The 49.5 cm length of the liquid xenon active region of the detector corresponds to 412 μ s at our operating field of 62 V/cm.

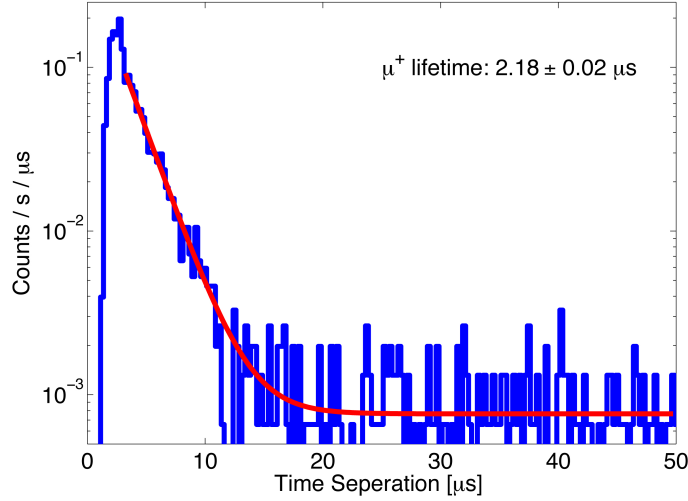


Figure 3: Positively-charged muon lifetime measured in zero-field data. We find agreement with the expected value of $2.197 \mu\text{s}$ [13].

3. Studies of the surface data

During both zero-field and dual-phase data-taking, we collected a number of useful datasets that allow us to study important properties of the detector, such as the xenon purity, the light collection, and the three-dimensional position reconstruction. In the dual-phase data we were able to use the γ background to measure a maximum electron drift length spanning half of the active length of the detector despite the non-optimal circulation path. The internal xenon circulation path was studied with a diagnostic ^{222}Rn injection into the detector, making use of the imaging properties of the TPC. The various backgrounds and radioactive sources used during surface operation, such as the cosmic muon background, cosmogenically-activated $^{129\text{m}}\text{Xe}$ and $^{131\text{m}}\text{Xe}$ isotopes, the α particles from the ^{222}Rn decay chain, and an external ^{137}Cs source, provided a wealth of opportunities to study the light

collection properties of the detector and tune the simulation developed for the LUX experiment. Finally, we have employed the ^{214}Bi - ^{214}Po near-coincident decays from the ^{222}Rn decay chain to study the resolution of the position reconstruction algorithms.

3.1. Xenon circulation and purification

The removal of electronegative impurities is essential to allow the electrons produced by ionization of the xenon atoms to drift away from the interaction site and for the scattering event to be reconstructed accurately along the 50 cm length of the active region of the LUX detector. Therefore, one of the goals of the surface commissioning of LUX was to obtain good detector purity as an essential exercise of the detector circulation systems in advance of the underground data-taking.

We used dual-phase data to estimate the electron attenuation in the active region of the detector. The decrease in S2 signal size as a function of drift time in the liquid, Δt , is described by an exponential function $S2 = \overline{S2}e^{-\Delta t/\tau}$, where τ is the mean lifetime that the electrons drift in the xenon before being captured by electronegative impurities and $\overline{S2}$ is the size of the S2 signal in perfectly pure xenon. After exploring several modes of circulation, we obtained an electron lifetime of $204 \pm 6 \mu\text{s}$, which was measured using background γ interactions with a single pair of S1 and S2 signals in the event window. In order to account for the fact that the γ 's are not mono-energetic, we normalize each measured S2 signal by its corresponding S1 signal, which was corrected for observed depth dependence and x-y position dependence through light response functions created for individual PMTs with the Mercury algorithm [15], discussed further in Sec. 3.3. The resulting trend in

(S2/S1), used to obtain the electron lifetime, is shown in Fig. 4. This lifetime corresponds to a drift length of 25 cm.

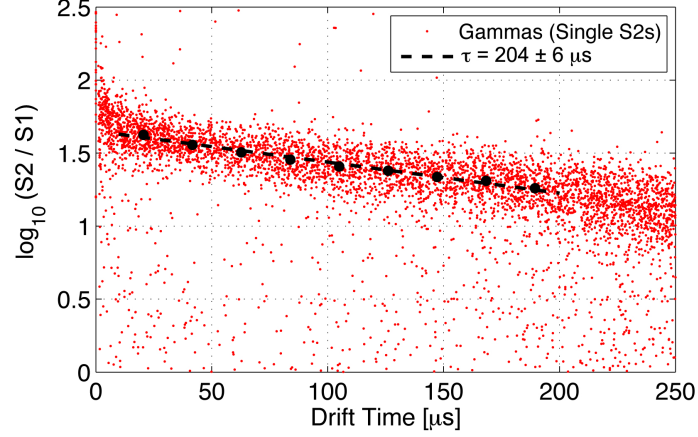


Figure 4: Highest measured electron lifetime, obtained using dual-phase γ -rays with a single pair of S1 and S2 signals in the event window. The circles indicate the means of the measured (S2/S1) ratio distribution in bins of drift time. The S1 signal in the event is corrected for observed depth dependence.

3.1.1. Imaging of the circulation path

In order to verify the nature of the compromise in the circulation path, 150 Bq of ^{222}Rn were injected into the detector through a cold trap to study the xenon flow, using the three α particles produced in the decays of ^{222}Rn (5.5 MeV), ^{218}Po (6.0 MeV), and ^{214}Po (7.7 MeV), shown in Fig. 5. The ^{222}Rn was introduced into the system through a port in the circulation path that is located before the getter so that the trace amount of impurities introduced via the additional plumbing would be prevented from reaching the detector. The ^{222}Rn source had a steady-state emanation rate of 1.42 Bq of ^{222}Rn per minute of gas flow through the port. Nitrogen was flown through the ^{222}Rn

source and into a cold trap that captured the ^{222}Rn . The amount of ^{222}Rn captured into the trap was controlled by the duration of nitrogen flow. Once the desired flow time was reached, the nitrogen flow was stopped, the ^{222}Rn source was valved off and the cold trap with ^{222}Rn was heated and introduced to the circulation path.

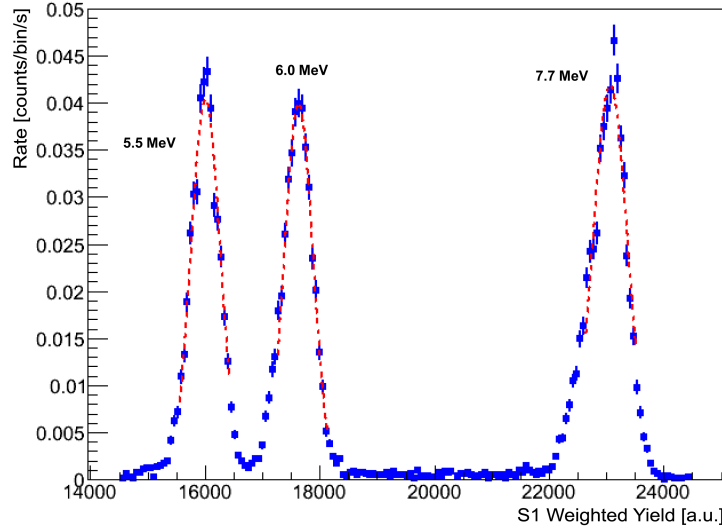


Figure 5: S1 pulse areas [arbitrary units] of the three α particles from the ^{222}Rn decay chain for zero-field data. The pulses are weighted to balance the light in the top and bottom PMTs, as described in Sec. 3.2.

By studying the ratio of light observed in the top PMT array relative to the bottom PMT array in zero-field data, we confirmed that the ^{222}Rn entered the detector in the second quadrant of the top PMT array. After ten minutes, the ^{222}Rn -doped xenon was seen to enter the bottom PMT array at the same location in the second quadrant, suggesting that the xenon was flowing down this side of the detector. This provided valuable diagnostic insight, as the intended circulation path would have introduced xenon at the bottom PMT

array in the first quadrant instead. Figure 6 shows the ^{222}Rn flow from the top of the detector to the bottom, at two of the time slices studied. A selection of 0.6 in the ratio of light in the top PMT array relative to bottom PMT array is applied to separate events as more “top-like” or “bottom-like”. Simulation indicates that the S1 light relative asymmetry $(S1_{top} - S1_{bottom})/(S1_{top} + S1_{bottom})$ provides a monotonic mapping to z -position, so the light ratio is a good proxy for depth.

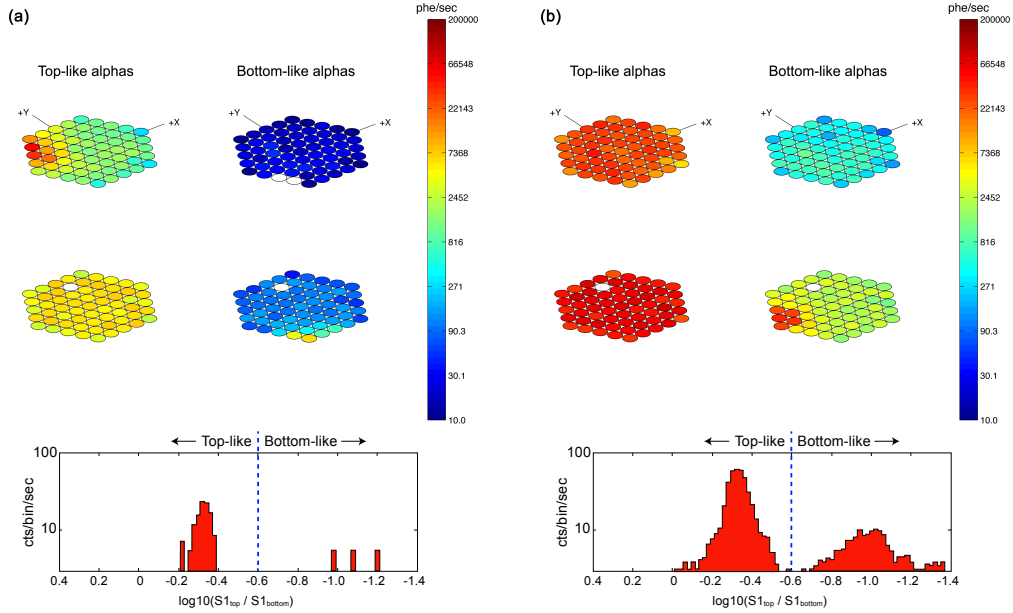


Figure 6: The average zero-field S1 signal hit patterns and S1 light ratio for α interactions in the LXe are shown at (a) 1.2 minutes and (b) 17 minutes after the ^{222}Rn injection.

It was expected and subsequently confirmed that this ^{222}Rn injection will not lead to significant backgrounds in a WIMP-search run. The radon-related background could arise from ^{210}Pb plate-out on the PTFE panels and other components, leading to low-energy interactions into the liquid bulk,

and from (α, n) neutron production on fluorine in the PTFE; a particular concern is the mis-reconstruction of the position of any surface interactions into the fiducial volume (nominally located approximately 50 mm from the surface of the panels). The latter effect could lead to mis-reconstruction of nuclear recoils from α interactions and electron recoils from β interactions, both of which may suffer incomplete charge extraction due to the proximity to the wall. Conservative calculations for these processes indicate that 150 Bq of ^{222}Rn will not compromise the WIMP sensitivity. For example, if all ^{222}Rn activity appeared as ^{210}Pb plated out onto the PTFE panels, the total neutron production rate from the (α, n) process would be 11 n/yr, assuming 10^{-5} n/ α on a thick fluorine target. This corresponds to 7.5% of neutron background expected from the PMTs, which are predicted to contribute a mere 0.04 WIMP-like background events in a nominal nuclear recoil search window of [5,25] keV after 30,000 kg-days.

3.2. *Light collection*

The light collection properties of the LUX detector are of utmost importance for the dark matter search, as they affect directly the size of the S1 signals and, consequently, our energy reach and background discrimination. In order to model the light collection properties of the detector, we use zero-field calibration data, which provides the best statistics in the S1 signal, to determine the number of detected phe per keV deposited through electron recoils in the xenon target. Two particularly important aspects of the light studies of the detector are the reflectivity of the PTFE panels in liquid xenon and the photoabsorption length for the 178 nm VUV scintillation photons. Liquid xenon can be purified to be highly transparent to its own scintillation

light and, consequently, the attenuation length for VUV photons depends on the xenon purity. This and other optical properties of the chamber can be obtained by detailed comparisons between real and simulated data.

The LUX detector is modeled with a GEANT4-based simulation [16, 17]. The simulation makes use of the NEST model [18], which takes into account the energy-, field-, and particle-dependent S1 and S2 signal yields, generating signals with realistic means and resolutions. While the detector geometry has been implemented accurately from direct detector measurements, a number of light collection properties of the detector must be determined from data. The unknown or uncertain parameters in the simulation include the reflectivity of the PTFE surfaces, the reflectivity of the wire planes, the photoabsorption length, the Rayleigh scattering length, and the reflectivity of the aluminum flashing deposited behind the quartz PMT windows. These quantities have been tuned separately for the gas and liquid regions of the detector through extensive comparisons with ^{137}Cs source data and then validated using the other available data.

The full ^{137}Cs energy deposition peak from the 662 keV γ -rays appears at 5624 ± 8 phe for a source located halfway down the active region, corresponding to 8.4 phe/keV, which is more than 2.5 times the zero-field value reported in Ref. [14] at the same energy. To obtain the best resolution on the 662 keV ^{137}Cs full energy deposition peak, the S1 signal pulse area measured in phe is weighted to correct for position-dependence of the light collection by rotating the distribution between light observed in the top and bottom PMTs to minimize the energy resolution. Three sets of optical parameters are tuned for both gas and liquid separately: the PTFE reflectivity, the photoabsorption

length, and the wire grid reflectivities. The light yield is determined from the data and the simulation is tuned to match both the light yield observed in data and the ratio of light in the top PMTs relative to the bottom PMTs. The simulation is rotated in an identical way. Figure 7 shows that excellent agreement has been achieved between the data and simulation for the ^{137}Cs source, which was contained in a 5 mm lead-backed collimator, lowered halfway down the length of the active region in a tube next to the cryostat. The resolution in the simulation is shown without any additional scaling or re-weighting, realistically replicating the resolution in data using only the NEST model. Through the tuning of the optical properties of the simula-

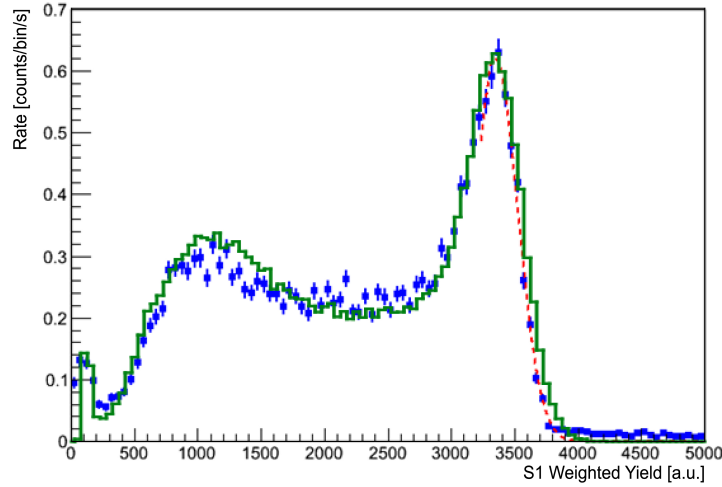


Figure 7: ^{137}Cs source S1 energy distribution [arbitrary units] for zero-field data. The S1 signal is rotated to balance the light between distribution in the top and bottom PMTs and minimize energy resolution. The S1 signal from the tuned simulation (histogram) is compared with data (points with errors) collected using a ^{137}Cs source located halfway down the length of the detector.

tion, we conclude that the hemispherical reflectivity of the PTFE panels is $> 95\%$ (pure Lambertian) in LXe and the photoabsorption length is at least 5 m in the liquid. The best description of our data is obtained with $100^{+0}_{-2}\%$ PTFE reflectivity and 11^{+2}_{-1} m photoabsorption length in LXe. The largest correlation between optical parameters is 2%. An accurate determination of these values is important for the thorough understanding of the LUX detector, as well as for the design of future experiments, and we will repeat these measurements in underground data-taking as well.

In order to confirm the validity of the light model obtained from the ^{137}Cs data, we have compared the tuned simulation with the 236 keV and 164 keV γ -rays from decays of $^{129\text{m}}\text{Xe}$ and $^{131\text{m}}\text{Xe}$, respectively. We find good agreement in the distribution of the data throughout the length of the detector, determined through the asymmetry of light in the top PMTs relative to the bottom PMTs, and in the energy resolution, shown in Fig. 8, which lends confidence to our light collection model. The simulation again replicates the resolution without additional scaling, even in the case of the non-monoenergetic 236 keV γ emission from $^{129\text{m}}\text{Xe}$, which consists of a 196 keV γ -ray plus a second 40 keV γ -ray. Using the simulation to inform the calculation of the volume-averaged light yield gives 8.2 ± 0.2 phe/keV for the xenon activation lines and 7.8 ± 0.2 phe/keV for the ^{137}Cs source for a fiducial volume of 100–150 kg, where systematic uncertainties are indicated.

In addition to the excellent light collection and high PTFE reflectivity we have observed, we also find good energy resolution at our calibration energies. We obtain $\sigma/E \sim 2\%$ for the three α particles, $\sim 5\%$ from the ^{137}Cs

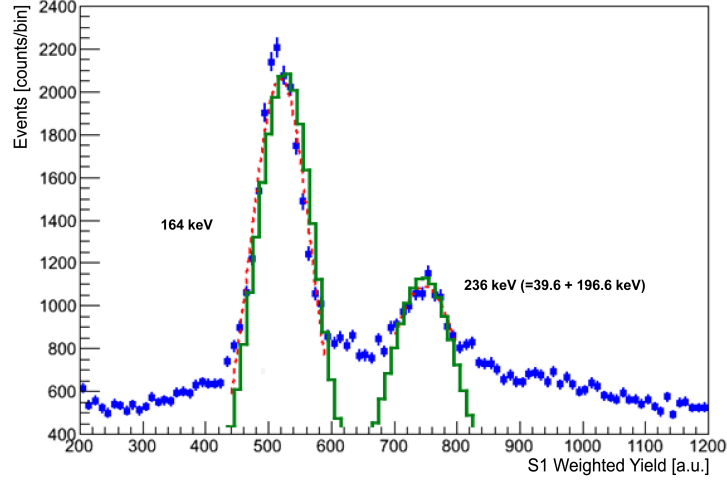


Figure 8: Zero-field S1 signals from the γ decay of cosmogenically activated $^{129\text{m}}\text{Xe}$ (236 keV) and $^{131\text{m}}\text{Xe}$ (164 keV) (arbitrary units). The resolution of the simulated S1 signal (histogram) agrees well with the data (points with error bars).

full energy deposition peak, and $\sim 10\%$ for the activated xenon γ -rays. All resolutions are measured using zero-field data. The energy resolutions as a function of energy are shown in Fig. 9. The resolutions have been obtained by correcting the S1 signals for z position-dependence.

3.3. Position reconstruction

We have explored x - y position reconstruction using the S2 signal in dual-phase data with several algorithms, including basic centroid methods. We have also implemented the Mercury vertex reconstruction algorithm developed for the ZEPLIN-III experiment, which provides precise x - y position information by measuring the light response of each PMT *in situ*. Figure 10 shows that we are able to resolve the 5 mm wire spacing in the gate wire

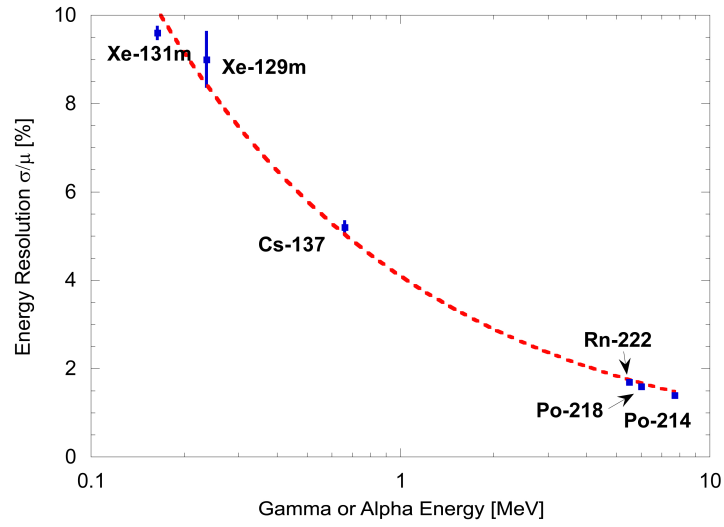


Figure 9: The energy resolution σ/E as a function of source energy for zero-field data. The data points are shown with error bars. We find a resolution of $\sim 2\%$ for the high-energy α particles, while we observe a $\sim 10\%$ resolution for the 164 keV γ -ray from the $^{131\text{m}}\text{Xe}$ decay. The trend in energy resolution is $\propto 1/\sqrt{E}$.

plane when applying the Mercury algorithm to background data; the individual wires appear as gaps because the electrons are focused around them in our electric field configuration. Owing to the lowered PMT gains, the energy of these reconstructed background events is generally well above that of the WIMP-search region.

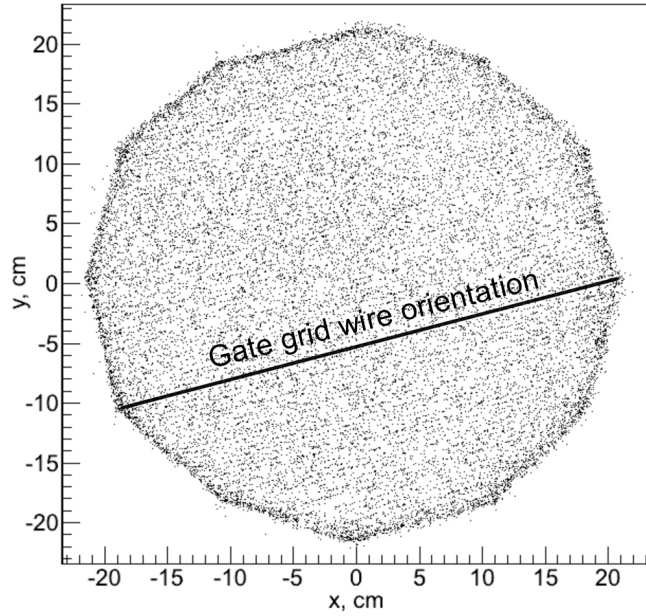


Figure 10: The x - y distribution of dual-phase background data reconstructed with the Mercury algorithm. The gaps indicate the position of the gate wires, which are separated by 5 mm and inclined at an angle of about 20° .

To study the statistical component of the position resolution using the Mercury reconstruction, we have used the 7.7 MeV α particle emitted in the ^{214}Po decay in delayed coincidence with the β decay of ^{214}Bi , which precedes the ^{214}Po decay with a half-life of 164.3 μs [19]. Since our event

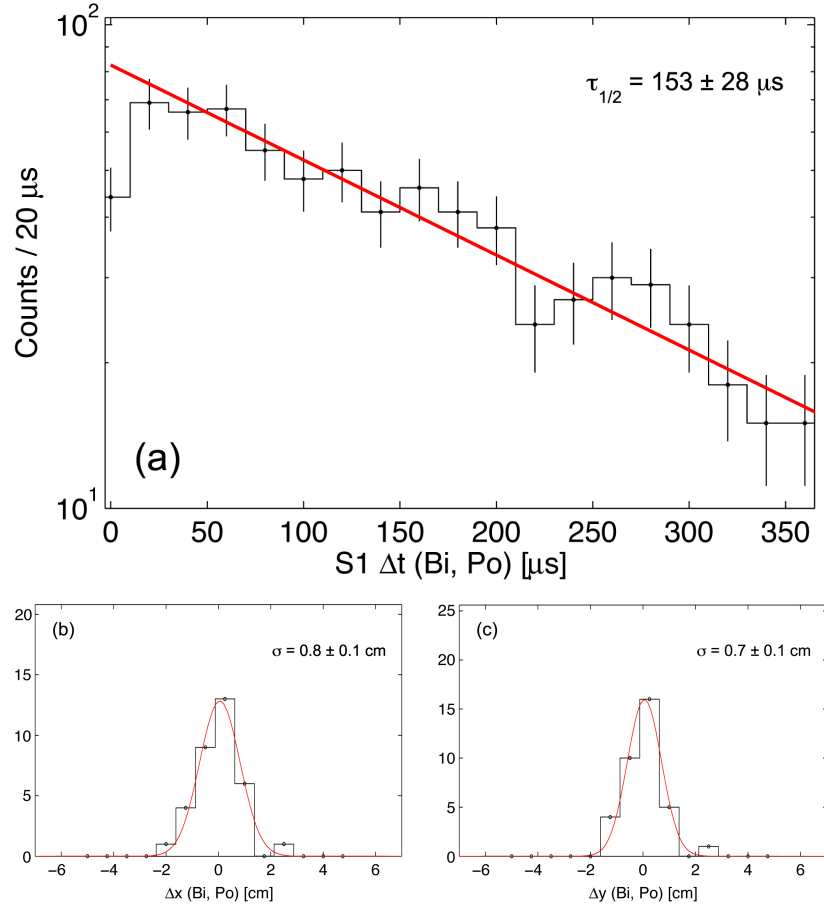


Figure 11: The ^{214}Bi - ^{214}Po candidates' (a) half-life and statistical resolution along (b) the x -axis and (c) the y -axis of the detector for dual-phase data. The reconstructed ^{214}Bi - ^{214}Po candidates show a half-life of $153 \pm 28 \mu\text{s}$, which is consistent with the expected half-life of $164.3 \mu\text{s}$ [19]. The statistical component of the resolution in either lateral direction is measured to be $\sigma \sim 7 \text{ mm}$.

window is 500 μs long, we can search for these two decays in the same event. In the reconstruction we require a pair of S1 and S2 signals followed by a second pair of S1 and S2 signals consistent with an α interaction. Using these events, we measure a half-life of $153 \pm 28 \mu\text{s}$, shown in Fig. 11, which is in good agreement with the known ^{214}Po half-life of 164.3 μs and confirms that the selection has identified a viable sample of ^{214}Bi - ^{214}Po coincident events. We then use the relative x and y positions of the two decays to estimate the statistical component of the resolution, finding $\sigma \sim 7 \text{ mm}$ in either direction for α particles distributed in the bulk of the LXe. This method treats the two sources as point-like, leading to an overestimate in the quoted resolution as the β track extends a few millimeters in the liquid. Since the ^{222}Rn decay daughters preferentially attach to the wire planes, we have also observed a population of α interactions from the gate wire plane (not shown in the figure); these have a much larger average S2 signal, as they are not suppressed by purity effects and there is no appreciable lateral diffusion of the signal since they are drifted only through the much higher extraction field in the LXe before they reach the liquid surface. These events have a resolution of approximately 3 mm in both the x and y direction.

4. Summary and Outlook

We have used the surface commissioning run of the LUX experiment to exercise all xenon detector systems and have demonstrated operational and readout capabilities. The surface run has also helped us to identify and address issues with the high-voltage delivery system, as well as to implement thorough checkouts of all systems. Benefiting from the wealth of experience

running and troubleshooting the detector operations, we have developed confidence in our ability to deploy the detector underground in a short period of time and to recommission it for full operation. We have taken advantage of the data collected to study the behavior of the xenon purification dynamics, the light collection of the detector, and to begin exploring event reconstruction algorithms, as well as to tune and validate our simulation using a variety of radioactive sources.

Using the tuned simulation we have updated the WIMP sensitivity estimates for $300 \text{ days} \times 100 \text{ kg}$ of data assuming zero background events and a minimum S1 signal threshold of 3 phe and an operating field of 500 V/cm. We have evaluated two scenarios in estimating our sensitivity, shown in Fig. 12: a conservative 15% average photon collection efficiency, replicating the state of the LUX detector at the end of the surface run, with a WIMP search range of nuclear recoil energies between 4.4-25 keV and 50% acceptance for nuclear recoils; and a more realistic light collection efficiency of 20%, which assumes full detector purification and a WIMP search range of 3.5-25 keV as measured in nuclear recoils and a 60% acceptance for nuclear recoils. The nuclear recoil energy is determined using the NEST model to obtain scaling of phe to nuclear recoil energy. In both cases we expect sensitivity at WIMP masses down to 10 GeV and in the realistic scenario we should be able to make a definitive statement on the CoGeNT result [20] under standard dark matter halo assumptions, assuming zero background events in the fiducial volume, and using straight-forward analysis techniques that place a firm 3 phe minimum threshold on the S1 signal and do not extrapolate to lower energies assuming statistical fluctuations upwards. We set the nuclear-recoil energy

scale to exactly zero at 3 keV, below which it is not possible to compare the NEST model with data [21–23]. We estimate a sensitivity to WIMP-nucleon cross sections in the realistic scenario better than $2 \times 10^{-46} \text{ cm}^2$ for a WIMP mass of $40 \text{ GeV}/c^2$, which exceeds the original LUX sensitivity goal.

When we begin underground operation in late 2012, the LUX experiment will become the largest two-phase xenon dark matter detector in the world and will represent the first xenon TPC deployed in a water shield. During the underground operation of LUX, we expect the best sensitivity to WIMP-nucleus scattering for WIMP masses above $8 \text{ GeV}/c^2$ in the realistic light collection scenario.

Acknowledgements

This work was partially supported by the U.S. Department of Energy (DOE) under award numbers DE-FG02-08ER41549, DE-FG02-91ER40688, DOE, DE-FG02-95ER40917, DE-FG02-91ER40674, DE-FG02-11ER41738, DE-FG02-11ER41751, DE-AC52-07NA27344, the U.S. National Science Foundation under award numbers PHYS-0750671, PHY-0801536, PHY-1004661, PHY-1102470, PHY-1003660, the Research Corporation grant RA0350, the Center for Ultra-low Background Experiments in the Dakotas (CUBED), and the South Dakota School of Mines and Technology (SDSMT). LIP-Coimbra acknowledges funding from Fundação para a Ciência e Tecnologia (FCT) through the project-grant CERN/FP/123610/2011. We gratefully acknowledge the logistical and technical support and the access to laboratory infrastructure provided to us by the Sanford Underground Research Facility (SURF) and its personnel at Lead, South Dakota.

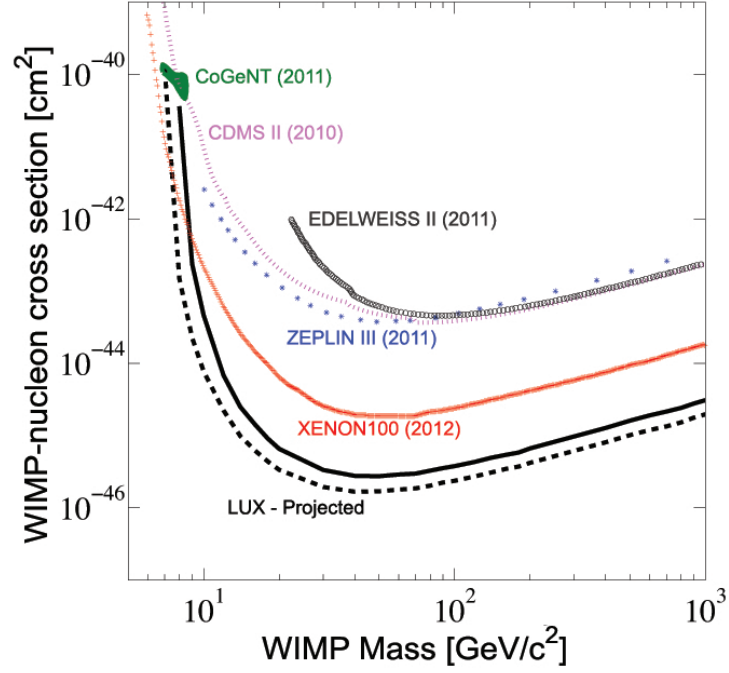


Figure 12: The projected LUX sensitivity at 90% CL is plotted in relation to other recent WIMP-nucleon scattering limits [20, 24–27]. The solid black line shows a limit assuming very conservative light collection and 30,000 kg-days of data without background, while the dashed black line shows a realistic estimate of the limit given our current understanding of the light collection and 30,000 kg-days of data.

References

- [1] M. W. Goodman, E. Witten, Detectability of certain dark matter candidates, *Phys. Rev. D* 31 (1985) 3059.
- [2] S. Fiorucci, et al., Status of the LUX dark matter search, *AIP Conf. Proc.* 1200 (2010) 977–980.
- [3] V. Chepel, H. Araújo, Liquid noble gas detectors for low energy particle physics, [arXiv:1207.2292](#).
- [4] D. Akerib, et al., The Large Underground Xenon (LUX) Experiment, Accepted for publication in *Nucl. Instrum. Meth. A*. [arXiv:1211.3788](#).
- [5] M. Yamashita, Y. Doke, K. Kawasaki, J. Kikuchi, S. Suzuki, Scintillation response of liquid xe surrounded by ptfe reflector for gamma rays, *Nucl. Instrum. Meth. A* 535 (2004) 692–698.
- [6] A. Bolozdynya, et al., Cryogenics for the LUX detector, *IEEE Trans. Nucl. Sci.* 56, Issue 4 (2009) 2309–2312.
- [7] A. Dobi, D. Leonard, C. Hall, L. Kaufman, T. Langford, et al., Study of a zirconium getter for purification of xenon gas, *Nucl. Instrum. Meth. A* 620 (2010) 594–598.
- [8] D. Leonard, A. Dobi, C. Hall, L. Kaufman, T. Langford, et al., A simple high-sensitivity technique for purity analysis of xenon gas, *Nucl. Instrum. Meth. A* 621 (2010) 678–684.
- [9] D. S. Akerib, et al., Data acquisition and readout system for the LUX dark matter experiment, *Nucl. Instrum. Meth. A* 668 (2012) 1–8.

- [10] D. Mei, A. Hime, Muon-induced background study for underground laboratories, *Phys. Rev. D* 73 (2006) 053004.
- [11] S. Kubota, M. Hishida, J.-z. Raun, Evidence for a triplet state of the self-trapped exciton states in liquid argon, krypton and xenon, *J. Phys. C* 11 (1978) 2645.
- [12] S. Kubota, M. Hishida, M. Suzuki, J.-z. Raun, Dynamical behavior of free electrons in the recombination process in liquid argon, krypton, and xenon, *Phys. Rev. B* 20 (1979) 3486.
- [13] J. Beringer, et al., Review of particle physics, *Phys. Rev. D* 86 (2012) 010001.
- [14] E. Aprile, et al., The XENON100 Dark Matter Experiment, *Astropart. Phys.* 35 (2012) 573–590.
- [15] V. N. Solovov, et al., Position reconstruction in a dual phase xenon scintillation detector, Accepted for publication in *IEEE Trans. Nucl. Sci.* [arXiv:1112.1481](#).
- [16] S. Agostinelli, et al., GEANT4: A Simulation toolkit, *Nucl. Instrum. Meth. A* 506 (2003) 250–303.
- [17] D. Akerib, X. Bai, S. Bedikian, E. Bernard, A. Bernstein, et al., LUXSim: A component-centric approach to low-background simulations, *Nucl. Instrum. Meth. A* 675 (2012) 63–77.
- [18] M. Szydagis, N. Barry, K. Kazkaz, J. Mock, D. Stolp, et al., NEST:

- A comprehensive model for scintillation yield in liquid xenon, JINST 6 (2011) P10002.
- [19] Y. Akovali, Nuclear data sheets for $a = 214$, Nuclear Data Sheets 76 (1) (1995) 127 – 190.
 - [20] C. Aalseth, P. Barbeau, J. Colaresi, J. Collar, J. Diaz Leon, et al., Search for an annual modulation in a p-type point contact germanium dark matter detector, Phys. Rev. Lett. 107 (2011) 141301.
 - [21] A. Manzur, A. Curioni, L. Kastens, D. McKinsey, K. Ni, et al., Scintillation efficiency and ionization yield of liquid xenon for mono-energetic nuclear recoils down to 4 keV, Phys. Rev. C 81 (2010) 025808.
 - [22] G. Plante, E. Aprile, R. Budnik, B. Choi, K. Giboni, et al., New Measurement of the Scintillation Efficiency of Low-Energy Nuclear Recoils in Liquid Xenon, Phys. Rev. C 84 (2011) 045805.
 - [23] M. Horn, V. Belov, D. Y. Akimov, H. Araujo, E. Barnes, et al., Nuclear recoil scintillation and ionisation yields in liquid xenon from ZEPLIN-III data, Phys. Lett. B705 (2011) 471–476.
 - [24] Z. Ahmed, et al., Dark matter search results from the CDMS II experiment, Science 327 (2010) 1619–1621.
 - [25] E. Armengaud, et al., Final results of the EDELWEISS-II WIMP search using a 4-kg array of cryogenic germanium detectors with interleaved electrodes, Phys. Lett. B702 (2011) 329–335.

- [26] D. Y. Akimov, H. Araujo, E. Barnes, V. Belov, A. Bewick, et al., WIMP-nucleon cross-section results from the second science run of ZEPLIN-III, Phys. Lett. B709 (2012) 14–20.
- [27] E. Aprile, et al., Dark Matter Results from 225 Live Days of XENON100 Data, Phys. Rev. Lett. 109 (2012) 181301.